OXFORD

Cerebral Cortex, 2024, **34**, bhad502
https://doi.org/10.1093/cercor/bhad502
Advance access publication date 13 January 2024
Original Article

Fibroblast growth factor 21 exerts a protective effect on diabetes-induced cognitive decline by remodeling cerebral glucose and neurotransmitter metabolism in mice

Xi Zhang[1,2,†], Hong Zheng[1,†], Zhitao Ni[1,†], Yuyin Shen[1], Die Wang[1], Wenqing Li[1,2], Liangcai Zhao[1,2], Chen Li[1,2,*], Hongchang Gao[1,2,3,*]

[1]Oujiang Laboratory (Zhejiang Lab for Regenerative Medicine, Vision and Brain Health), School of Pharmaceutical Sciences, Wenzhou Medical University, Wenzhou 325035, China
[2]Key Laboratory of Efficacy Evaluation of Traditional Chinese Medicine and Encephalopathy Research of Zhejiang Province, Wenzhou Medical University, Wenzhou 325035, China
[3]Institute of Aging, Key Laboratory of Alzheimer's Disease of Zhejiang Province, Wenzhou Medical University, Wenzhou 325035, China

*Corresponding authors: Email: lichen2zh@163.com, gaohc27@wmu.edu.cn

[†]Xi Zhang, Hong Zheng, and Zhitao Ni contributed equally to this work.

Diabetes mellitus (DM) causes damage to the central nervous system, resulting in cognitive impairment. Fibroblast growth factor 21 (FGF21) exhibits the potential to alleviate neurodegeneration. However, the therapeutic effect of intracerebroventricular (i.c.v) FGF21 infusion on diabetes-induced cognitive decline (DICD) and its potential mechanisms remain unclear. In this study, the impact of FGF21 on DICD was explored, and ^{1}H nuclear magnetic resonance (NMR)-based metabolomics plus ^{13}C NMR spectroscopy in combine with intravenous [1-^{13}C]-glucose infusion were used to investigate the underlying metabolic mechanism. Results revealed that i.c.v FGF21 infusion effectively improved learning and memory performance of DICD mice; neuron loss and apoptosis in hippocampus and cortex were significantly blocked, suggesting a potential neuroprotective role of FGF21 in DICD. Metabolomics results revealed that FGF21 modulated DICD metabolic alterations related to glucose and neurotransmitter metabolism, which are characterized by distinct recovered enrichment of [3-^{13}C]-lactate, [3-^{13}C]-aspartate, [4-^{13}C]-glutamine, [3-^{13}C]-glutamine, [4-^{13}C]-glutamate, and [4-^{13}C]-γ-aminobutyric acid (GABA) from [1-^{13}C]-glucose. Moreover, diabetes-induced neuron injury and metabolic dysfunctions might be mediated by PI3K/AKT/GSK-3β signaling pathway inactivation in the hippocampus and cortex, which were activated by i.c.v injection of FGF21. These findings indicate that i.c.v FGF21 infusion exerts its neuroprotective effect on DICD by remodeling cerebral glucose and neurotransmitter metabolism by activating the PI3K/AKT/GSK-3β signaling pathway.

Key words: FGF21; metabolomics; neurotransmitter; 13C NMR spectroscopy.

Introduction

Diabetes mellitus (DM), a frequently observed metabolic syndrome with elevated blood glucose levels, has become the primary cause of mortality and morbidity worldwide (Ngo et al. 2020). DM may induce various complications and increase patients' risk of premature death. Notably, diabetes-induced cognitive decline (DICD) is one of the central nervous system (CNS) complications of DM that causes structural and neurophysiological damage in several domains of the brain (Musen et al. 2018), consequently leading to impairment of memory, language, and judgment (Brismar et al. 2007). Several pathological factors for DICD have been proposed, such as oxidative stress (Zheng et al. 2018b), inflammation (Cui et al. 2021), autophagy dysregulation (Wu et al. 2019; Zhang et al. 2021), and neuronal apoptosis (Kong et al. 2018). In addition, metabolic abnormalities represent a critical pathogenic factor for DICD. An efficient treatment for DICD is lacking; therefore, understanding the systemic metabolic mechanisms of DICD is essential for discovering novel therapeutic agents.

Fibroblast growth factor 21 (FGF21), a crucial endocrine FGF family member, regulates cell survival and growth (Adams et al. 2012). FGF21 plays multifarious roles in insulin sensitivity and glucose and lipid homeostasis (Lin et al. 2013; BonDurant and Potthoff 2018; Byun et al. 2020). In addition to its metabolic actions in its primary target tissues, FGF21 has been reported to be a remarkable neuroprotective factor in neurodegeneration. For example, FGF21 treatment can effectively attenuate brain cell apoptosis and ameliorate impaired cognition in rats with insulin resistance (Sa-Nguanmoo et al. 2016). FGF21 protects the neurons against oxygen–glucose deprivation-induced brain injury, possibly by promoting neuronal survival through PI3K/AKT signaling pathway activation (Ye et al. 2019), indicating that FGF21 might have a role in propitious functional recovery after neonatal brain injury. Most importantly, FGF21 improves metabolic homeostasis in diabetes (Dutchak et al. 2012) and has been reported to be safe and effective in clinical studies (Geng et al. 2020; Watanabe et al. 2020). Besides, as a potential therapeutic medicine for CNS diseases (Hsuchou et al. 2007), the half-life of recombinant FGF21

Received: July 9, 2023. **Revised:** November 29, 2023. **Accepted:** November 30, 2023

in rodents is short (Kharitonenkov et al. 2007), daily or twice-daily administration is required to achieve desired pharmacological effects (Veniant et al. 2012). Several studies have confirmed to measure the steady-state effects of FGF21 on DICD after chronic administration or after transgenic overexpression throughout the development (Xu et al. 2009). In our previous study, we also had proved that FGF21 significantly improved the learning and memory defects of DICD mice, which were received recombinant FGF21 (2 mg/kg, i.p.) daily for four consecutive weeks (Zhao et al. 2022). However, limited information is available on the pharmacological effect of a single intracerebroventricular (i.c.v) injection of FGF21 on DICD.

Nuclear magnetic resonance (NMR)–based metabolomics analysis represents a crucial platform for identifying the global metabolic information related to pathological conditions (Nicholson et al. 1999). Metabolomics has exhibited its potential for exploring metabolic abnormalities in diabetes-related brain diseases (Ivanisevic and Siuzdak 2015). Our previous study had detected metabolic changes in diverse brain regions of DM rats (Zheng et al. 2017a) and db/db mice (Zheng et al. 2017c) with impaired cognition; results revealed that cognitive decline is possibly associated with various metabolic alterations in the brain. Additionally, the ^{13}C NMR approach is a powerful analytical tool for tracing metabolic fate and quantifying metabolic changes with high sensitivity by using ^{13}C-labeled metabolic substrate injection (Shulman et al. 1990; Choi et al. 2019). Recently, ^{13}C NMR metabolomics has been successfully developed to explore the metabolic mechanism underlying several neurodegenerative disorders. For instance, by adopting ^{13}C NMR plus intravenous [1-^{13}C]-glucose infusion, Zhou et al. (2018) found a decrease in glucose utilization and a reduction in lactate–alanine shuttle neurotransmitter/energy metabolism in the brain regions of amyloid pathology APP/PS1 mice. Additionally, an ex vivo ^{13}C NMR approach plus intravenous [1-^{13}C]-glucose and [2-^{13}C]-acetate infusions were used to explore brain metabolism during type 1 diabetes (Wang et al. 2015). Furthermore, our previous study reported that an unbalanced neuron–astrocyte cooperation metabolism and disruptive gluconeogenesis might be linked to the cognitive decline in type 2 diabetes by using ^{13}C NMR metabolomics plus [2-^{13}C]-acetate and [3-^{13}C]-lactate infusions (Zheng et al. 2017b). Hence, integrating the ^{1}H NMR-based metabolomics analysis and the ^{13}C NMR approach may be useful in exploring the metabolic mechanisms related to FGF21's protective effect on DICD.

In the current study, the metabolic profiles in brain tissues of DICD mice following i.c.v FGF21 infusion were examined by ^{1}H NMR-based metabolomic approach, and metabolic fates were traced through ^{13}C NMR approach plus [1-^{13}C]-glucose infusion. The present study aims to characterize the efficacy and metabolic changes of i.c.v injection of FGF21 in DICD and elucidate the underlying metabolic and therapeutic mechanisms.

Materials and methods

Animals

A 6-wk-old male C57BL/6J mice (n = 12 for each group, body weight = 18 ± 5 g) was purchased from SLAC Laboratory Animal Corporation (Shanghai, China) and housed in the SPF condition under controlled humidity/temperature and 12-h light/dark cycle at the Laboratory Animal Center of Wenzhou Medical University. All mice were allowed to receive standard chow and drink water. All experiments were performed according to the ethical policies and procedures approved by the Institutional Animal Care and Use Committee of Wenzhou Medical University (ID number: wydw-2020-0124).

Streptozocin-induced diabetic mice

All mice were acclimatized for 1 wk and then randomly assigned into three groups: healthy controls (Con), DICD, and FGF21 group (n = 6 for each group). After starving for 12 h, mice in DICD and FGF21 groups were injected intraperitoneally with streptozocin (STZ, Sigma-Aldrich, St. Louis, MO) for five consecutive days, and the optimum dose was determined to be 50 mg/kg of the body weight. The STZ powder was prepared in a 0.1% sodium citrate buffer (pH = 4.5). Sodium citrate buffer in identical volumes was administered to Con mice. The blood glucose content in the tail vein was measured by using a handheld glucometer (Roche, Basel, Switzerland) at day 3 after STZ injection. The mice exhibiting a fasting blood glucose level > 11.1 mmol/L were considered to have diabetes.

Morris water-maze test

According to our previous studies, diabetic mice showed cognitive dysfunction after 12 wk after STZ injection (Gao et al. 2019; Xiong et al. 2023). Hence, the Morris water-maze (MWM) test was conducted to examine cognitive function of mice after 12 wk of STZ treatment, as described previously (Zheng et al. 2021). Briefly, we divided a round white pool (depth and diameter of 50 and 100 cm, respectively) containing opaque water (23 °C ± 1 °C) into four equivalent quadrants and placed a circular escape platform 1 cm below water within the center of a quadrant. During a 4-day continual training period, the mice were guided to search and stand on the platform when they could not find it within 60 s. Finally, on day 5, each trained mouse underwent a 90-s probe test in a similar starting position without an escape platform. The escape latency in the training stage, number of target crossings, time spent within the target quadrant, and swimming length/speed in the target area during the trial phase were recorded and determined using Viewer 2 software (Biobserve GmbH, Bonn, Germany).

I.c.v injection of recombinant FGF21

All i.c.v injection procedures and the dose of FGF21 herein were performed according to previous studies (Scarlett et al. 2016; Santoso et al. 2017; Chao et al. 2019). In brief, mice were fixed on the stereotaxic instrument (RWD Life Science, Shenzhen, China) after isoflurane anesthesia treatment. A small portion of the skin was cut to expose the skull, and a hole was drilled in the skull, through which one 32-gauge needle was implanted in the right lateral ventricle on the following coordinates: 1.5 mm lateral to the bregma, 0.6 mm posterior, and 1.7 mm deep. Recombinant FGF21 (3 μg, Cloud-Clone Corp, Wuhan, China) was dissolved in saline at a dose of 1 $\mu g/\mu L$ and i.c.v-injected into the DICD mice by using a microinfusion pump at the rate of 0.2 μL/20 s. Thereafter, the needle was removed with no blood reflux following 2-min dwelling, the burr hole was filled with bone wax, and the skin was sutured. Finally, isoflurane flux was interrupted, and the mice were allowed to recover for 1 wk to conduct further experiments. The mice in Con and DICD group were i.c.v-injected the same volume of saline in the same way.

Intravenous [1-^{13}C]-glucose infusion

After overnight fasting, all mice were anesthetized with isoflurane and placed on the temperature-controlled pad to maintain their rectal temperature between 36.8 °C and 37.5 °C. [1-^{13}C]-glucose (Sigma-Aldrich, >99% pure) solution was prepared in saline at a concentration of 0.5 mol/L. The left jugular vein was dissected,

and [1-^{13}C]-glucose solution was constantly injected into the left jugular vein through the microinfusion pump for a 30-min period at 0.1 mL/kg/min rate, according to a previous study (Zhou et al. 2018). Then, the blood glucose contents in the tail vein before and after injection were determined using a handheld glucometer. After 15-min infusion, mice were sacrificed by decapitation, and the brain tissues were rapidly isolated and frozen in liquid nitrogen and then kept at −80 °C.

Nissl staining

For histological examination, the brain tissues were harvested and fixed in 10% formalin buffer for 24 h, followed by gradient ethanol dehydration, paraffin embedding, and slicing into 5-μm sections. After washing the section thrice with distilled water, we dehydrated each section in 100% ethanol, followed by xylene transparentizing and neutral resin covering. Later, each section was dehydrated and stained using pre-warmed (56 °C) 0.5% cresyl violet solution for 1 h. The morphological alterations of Nissl bodies were observed and captured under an upright microscope (ECLIPSE Ni, Nikon, Tokyo, Japan).

Cell culture and treatment

The SH-SY5Y cells were purchased from Shanghai Institute of Biochemistry and Cell Biology (Shanghai, China) and cultured in the DMEM/F12 medium (Gibco, Thermo Fisher Scientific, Waltham, USA) with 10% fetal bovine serum and 1% penicillin-streptomycin (Gibco) under 5% CO_2 and 37°C conditions. Later, we divided the cells into three groups, namely, the normal glucose group (NG, 5.5 mM), the high glucose group (HG, 50 mM), and the FGF21-treated group (50 mM of glucose supplemented with 100 ng/mL of FGF21).

Cell counting kit-8 assay

A cell counting kit-8 (CCK8) assay was conducted to measure cell viability using CCK8 reagents (cat# CK04, Dojindo, Kumamoto, Japan). The cells (5×10^3/well) were inoculated in 96-well plates for 12 h. After removing the medium, the cells were rinsed twice using 200 μL of PBS solution before adding the treatment medium at the indicated time points. Then, CCK8 reagents (10 μL) were placed into each well for 2-h incubation at 37 °C. Finally, cell viability was calculated by determining the absorbance (OD value) at 450 nm using the SpectraMax 190 Microplate Reader (MD, San Francisco, USA).

Hoechst 33342 nuclear staining

The SH-SYSY cells (1×10^6 cells/well) were incubated in a 6-well chamber slide coated with poly-L-lysine and cultured in the indicated medium for 4 days. After 45-min fixation by 4% paraformaldehyde (PFA) at 4 °C, the cells were rinsed thrice using PBS, followed by 5-min staining with Hoechst 33342 (cat# C1025, Beyotime Biotech, Nantong, China) in the dark. After rinsing with PBS thrice, the images were captured using a microscope (ECLIPSE Ni, Nikon, Tokyo, Japan) and processed by Image J software (V 1.47, National Institutes of Health, Bethesda, MD, USA).

Western blot analysis

The brain tissues (hippocampus and cortex) and SH-SYSY cells were harvested and homogenized by using lysis buffer (Beyotime Biotech, Nantong, China) containing a protease/phosphatase inhibitor cocktail (Beyotime Biotech), followed by 20-min centrifugation at 12,000 g and 4 °C and supernatant collection. The protein concentrations of samples were determined using the BCA protein detection kit (Beyotime Biotech). The proteins of samples were separated on 8% or 10% SDS-PAGE gel and then transferred onto the PVDF membrane (Immobilon-P Transfer Membrane, Merck Millipore, Billerica, USA). After 2-h blocking using 5% BSA, the membranes were incubated overnight with primary antibodies at 4 °C, followed by washing thrice with TBST (TBS with 0.05% tween 20) and incubated for 1 h with secondary antibodies (1:5,000, Affinity Biosciences, Changzhou, China) under ambient temperature. Then, the immunoreactivity was visualized by using a chemiluminescence (ECL) kit (Merck Millipore, Billeria, USA) on the ChemiDocXRS Imaging system (Bio-Rad, Hercules, USA). Protein expressions were normalized to respective protein controls, followed by quantification by ImageJ software. Primary antibodies used in the study are as follows: β-actin (1:1,000, CST, Boston, USA), GAPDH (1:1,000, CST, Boston, USA), Bax (1:1,000, Proteintech, Chicago, USA), Bcl-2 (1:1,000, Proteintech, Chicago, USA), caspase-3 (1:1,000, CST, Boston, USA), AKT (1:1,000, CST, Boston, USA), phospho-AKT (1:1,000, CST, Boston, USA), PI3K (1:1,000, CST, Boston, USA), phospho-PI3K (1:1,000, CST, Boston, USA), GSK3-β (1:1,000, CST, Boston, USA), and phospho-GSK3-β (1:1,000, CST, Boston, USA).

NMR sample preparation

To extract metabolites from whole brain homogenates, we homogenized the whole brain tissues with prechilled methanol (4 mL/g) and prechilled water (0.85 mL/g) by using the handheld electric homogenizer (FLUKO, Shanghai, China), as reported in our prior study (Zheng et al. 2018a). Next, we homogenized the resultant mixture with prechilled methanol (2 mL/g) and prechilled water (2 mL/g). Afterwards, we vortexed the resultant mixture for 20 s, followed by 15-min centrifugation at 12,000 g at 4 °C. After collection, we lyophilized the supernatants for a 24-h period, followed by preservation at −80 °C before use.

NMR-based metabolomics analysis

Lyophilized extracts from the brain tissues were soaked in D_2O (500 μL) containing 0.05% sodium trimethylsilyl propionate-d_4 (TSP, 0.42 mM) and then transferred into the 5-mm NMR tube. The ^{1}H-NMR spectra were obtained by the Bruker AVANCE III 600 MHz NMR spectrometer (Bruker Biospin, Rheinstetten, Germany) with a TXI probe at 298 K. The normalized single-pulse sequence containing water signal presaturation, "ZGPR," was adopted to obtain the ^{1}H-NMR spectra. The main parameters were acquisition time = 2.66 s/scan; spectral width = 12,335.5 Hz; scans = 256; relaxation delay = 4 s; and data points = 256 K.

All ^{1}H-NMR spectra were corrected according to the baseline and phase and calibrated them based on the lactate methyl peak (CH3, 1.33 ppm) using Topspin 3.0 (Bruker, Rheinstetten, Germany). Then, an "icoshift" process was conducted to align NMR spectra based on MATLAB software (R2012a, The MathWorks Inc., MA, USA). The spectral regions at 0.0–9.0 ppm, excluding the residual water signal (4.7–5.6 ppm), were then segmented and integrated them into the binning data at the 0.01-ppm interval. The metabolites were assigned according to the Human Metabolome Database and Chenomx NMR suite 7.0 (Chenomx Inc., Edmonton, AB, Canada) (Wishart et al. 2018).

^{13}C-NMR analysis

The ^{13}C-NMR spectra were recorded by using the Bruker AVANCE III 600 MHz NMR spectrometer (Bruker Biospin, Rheinstetten, Germany) operating at 298 K and 150.92 (C) MHz. Additionally, the inverse-gated decoupling sequence, "INVGATE," was used to obtain the ^{13}C-NMR spectra to avoid the nuclear Overhauser effect. The main parameters were flip angle = 30°; spectral width = 33,333 Hz; scans = 32,768; data points = 64 K; delay time = 2 s; and acquisition time = 1 s/scan. The chemical shift of lactate (21.9 ppm) was used as a reference for the ^{13}C data calibration. The

^{13}C-NMR signals were assigned according to our published results (Wang et al. 2015; Zheng et al. 2017b; Zhou et al. 2018). Following [1-^{13}C]-glucose infusions, specific metabolite ^{13}C-enrichment was determined according to ^{13}C natural abundance (1.1%).

Statistical analysis

All mice were randomly assigned into experimental groups in the current study. The orthogonal partial least squares discriminant analysis (OPLS-DA) and partial least squares discriminant analysis (PLS-DA) models were adopted to obtain metabolic pattern changes among various groups based on ^{1}H-NMR and ^{13}C-NMR data by using SIMCA 12.0 (Umetrics, Umeå, Sweden). All values are displayed in the form of mean ± SD. We analyzed time-series data through the repeated measure analysis. The significance of difference among three groups was analyzed by using ANOVA with a Bonferroni-adjusted test for pairwise comparisons. Metabolic pathways were manually drawn by CorelDRAW Graphics Suite (Corel Inc., Ottawa, Canada) based on KEGG pathways (www.genome.jp/kegg/) and the Small Molecule Pathway Database (SMPDB, www.smpdb.ca/). A P-value of <0.05 denoted statistical significance.

Results

FGF21 treatment protected against cognitive dysfunction of DICD mice

We performed the MWM test at weeks 12 and 15 after STZ treatment to examine cognitive function of mice (Fig. 1A). After 12 wk of STZ injection, DM mice with impaired learning and memory abilities were considered for subsequent study. As shown in Fig. 1B, the escape latency of DICD mice dramatically increased compared with that of Con group, which declined after i.c.v injection of FGF21, suggesting that FGF21 treatment remarkably rescued the impaired learning ability of DICD mice. After 4-day training, we removed the escape platform for assessing mouse memory ability. Swimming trajectories are shown in Fig. 1C. The crossing number at the initial platform position (Fig. 1D), time (Fig. 1E) and distance (Fig. 1F) in the goal area, and total swimming length percentage (Fig. 1G) in the target quadrant were remarkably decreased in the DICD mice compared with those in Con. However, such behavioral performances significantly increased following FGF21 treatment. These findings revealed that FGF21 effectively alleviated the cognitive deficits of DICD mice.

Pathological effect of FGF21 treatment on the neurons of DICD mice

To examine the histological effect of FGF21 on the DICD mice, Nissl staining was conducted to determine the number of surviving neurons in the hippocampus and cortex of mice. As illustrated in Fig. 2A, the neuron cell numbers were remarkably decreased in cornu ammonis area 1 (CA1), cornu ammonis area 3 (CA3) and dentate gyrus (DG) regions of the hippocampus of DICD mice relative to those of normal mice; however, the number of neurons were increased after i.c.v FGF21 treatment. Consistently, the number of surviving neurons in the cortex of DICD mice were significantly decreased, whereas cortical neuron loss was attenuated by i.c.v FGF21 treatment, as shown in Fig. 2B. Subsequently, we analyzed the role of FGF21 exposure in SH-SY5Y cells, the human neuroblastoma cell line extensively adopted to study neuronal function in vitro (Fig. 3). The CCK8 assay revealed that 50-mM HG exposure significantly decreased the cell viability from day 3 (Fig. 3A). However, the reduced cell viability was markedly reversed by the treatment with 100 ng/mL FGF21 from day 4. Hence, day 4 was selected as a time reference for subsequent analysis. Hoechst nuclear staining, utilized for assessing the condensed chromatin in apoptotic cells, revealed that HG exposure for 4 days significantly induced cell apoptosis (Fig. 3B and C). However, FGF21 markedly repressed HG-induced upregulation of apoptosis, which manifested as decreased nuclear condensation of the chromatin and the shrinkage of nuclei (Fig. 3B and C). These results were validated by conducting a western blot assay on pro-apoptotic proteins (caspase-3, cleaved caspase-3) and deriving the Bax/Bcl-2 ratio. These apoptotic markers were increased under HG conditions but decreased after FGF21 treatment (Fig. 3D–F).

Neuroinflammation plays a crucial role in the development of cognitive decline, as it is also implicated in more chronic forms of neurodegeneration (Ransohoff 2016). Besides, FGF21 and its analog LY2405319 are generally considered to be related with immunogenicity (Gaich et al. 2013; Kang et al. 2020). We thus examined the inflammatory response of FGF21 on DICD. Results showed that the messenger RNA (mRNA) levels of inhibited pro-inflammatory cytokines (IL-1β, IL-6, and TNFα) and promoted anti-inflammatory cytokines (IL-4 and IL-10) in DICD were not altered by i.c.v FGF21 treatment (Supplementary Fig. 1A). Additionally, i.c.v FGF21 treatment also failed to alter the elevated IL-6 and decreased IL-10 protein levels in brain of DICD (Supplementary Fig. 1B). Thus, our results demonstrated that i.c.v FGF21 treatment effectively ameliorated neuron loss and apoptosis of DICD mice, but not inflammation.

Metabolic changes of FGF21 in the brain of DICD mice

To investigate the metabolic mechanism underlying the neuroprotective effect of FGF21 on DICD, an ^{1}H NMR-based metabolomics approach was used to analyze the metabolic alterations of brain tissues in the DICD mice. Figure 4A illustrates the representative ^{1}H-NMR spectra of brain tissues from all three groups. We identified diverse metabolites, which were mainly involved in amino acid metabolism (valine, leucine, alanine, and isoleucine), energy metabolism (succinate [Suc], lactate, fumarate, glucose, creatine, ADP, and AMP), astrocyte–neuron metabolism (N-acetyl aspartate [NAA], myo-inositol, and taurine [Tau]), neurotransmitter metabolism (γ-aminobutyric acid [GABA], aspartate [Asp], glutamine, and glutamate), choline metabolism (choline), and other metabolites (inosine). The corresponding resonance assignments with chemical shifts of metabolites in ^{1}H NMR spectra are shown in Supplementary Table 1. The PLS-DA model was adopted to discriminate the metabolic pattern changes among Con, DICD, and FGF21-treated mice. As illustrated in Fig. 4B, the PLS-DA score plot revealed a clear metabolic pattern separation among the three groups. Subsequently, the OPLS-DA model was employed to characterize the discrimination between the two groups. Figure 4C illustrates an apparent separation between Con and DICD mice on brain metabolome, and its corresponding loading plot showed a series of metabolites that mainly attributed to this separation, including glutamate, GABA, NAA, and glucose (Fig. 4D). A clear metabolic pattern separation between DICD and FGF21-treated mice is illustrated in Fig. 4E, and this metabolic separation might be attributed to lactate, NAA, glutamate, Tau, and glucose levels (Fig. 4F). Afterward, an ANOVA with a Bonferroni-adjusted test for pairwise comparisons was conducted to identify metabolic differences among three groups; the difference was considered to be statistically significant when $P < 0.05$. As shown in Fig. 4G, glucose, lactate, GABA, glutamate, NAA, and Asp were identified as differential metabolites between the Con and DICD mice. The differences between the DICD and FGF21-treated mice were statistically significant regarding glucose, lactate, GABA, glutamate, NAA, Asp, ADP, and Tau levels (Fig. 4H).

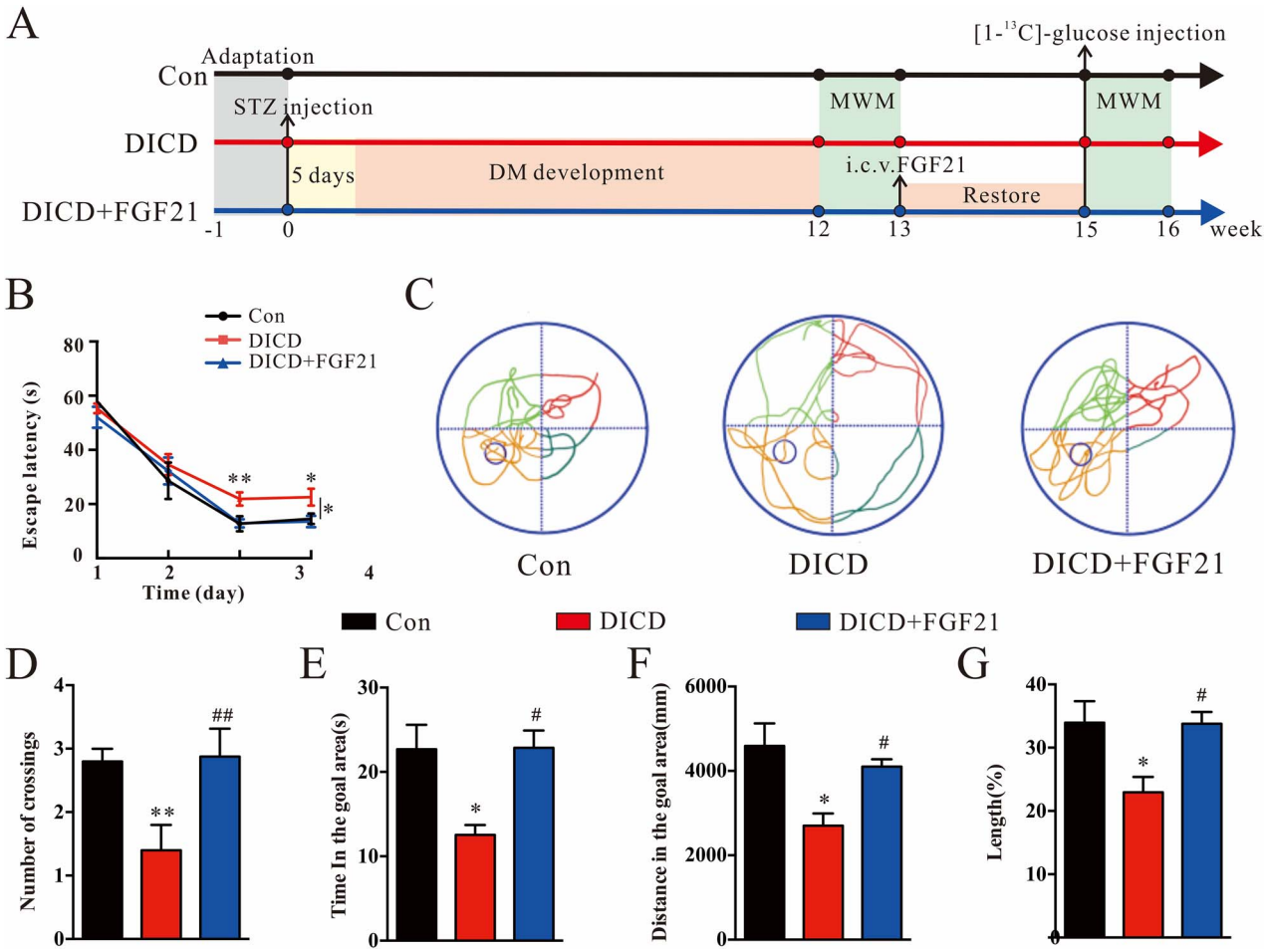

Fig. 1. FGF21 mitigates cognitive deficits in DICD mice. (A) After 1 wk of acclimation, diabetes was induced in the mice by intraperitoneally injecting STZ consecutively for 5 days, and the MWM was conducted to determine the DM mice's cognitive function at week 12 after STZ treatment. When the DM mice exhibited impaired cognitive functions, 3 μg of FGF21 was administered to the DICD mice through i.c.v administration. After a 2-wk restoration period, [1-^{13}C]-glucose was continually injected into the mice through the left jugular veins, and MWM was performed to test the learning/memory abilities of the DICD mice after FGF21 treatment ($n = 6$). (B) Escape latency during the 4-day training period of MWM test. (C) A swimming path was used for the probe test on the fifth day. (D) Crossing number at the initial platform position, (E) time, (F) distance in the goal area, and (G) swimming length percentage within the target quadrant. Data are expressed as the mean ± SD. The significance of difference among three groups was analyzed by using ANOVA with a Bonferroni-adjusted test for pairwise comparisons. $^{*}P < 0.05$, $^{**}P < 0.01$, $^{***}P < 0.001$ vs. normal mice; $^{\#}P < 0.05$, $^{\#\#}P < 0.01$, $^{\#\#\#}P < 0.001$ vs. DICD mice.

To further characterize the metabolic changes of i.c.v FGF21 treatment in DICD, the changes of the common differential metabolites were detected, as shown in Fig. 4I–N. FGF21 treatment remodeled the metabolic alterations of brain in the DICD mice, mainly involved in glucose and neurotransmitter metabolism. The elevated lactate and glucose contents were detected in the brain of DICD mice relative to those in the normal mice, which were declined dramatically following i.c.v FGF21 injection (Fig. 4I and J). Compared with Con mice, lower levels of neurotransmitters (GABA, glutamate, and Asp) and a marker for neuronal viability (NAA) in DICD mice were significantly increased after FGF21 treatment (Fig. 4K–N). In conclusion, FGF21 modulated the metabolic dysfunction of DICD, which mainly related to glucose and neurotransmitter metabolism.

Glucose metabolic fate in the brain of DICD mice after FGF21 treatment

To trace the metabolic fate of brain glucose metabolism, the ^{13}C NMR-based metabolomics plus intravenous [1-^{13}C]-glucose infusion was conducted. Figure 5A illustrates a representative ^{13}C NMR spectrum for brain tissue of normal mice after [1-^{13}C]-glucose infusion. Clearly, ^{13}C isotope was successfully added to specific carbon sites of various metabolites, including alanine (Ala: C3, δ17.0), lactate (Lac: C2, δ69.4; C3, δ21.0), GABA (C2, δ35.3; C3, δ24.5; C4, δ40.2), NAA (C2, δ54.1; C3, δ40.5; C6, δ22.8), glutamine (Gln: C2, δ55.0; C3, δ27.1; C4, δ31.7), glutamate (Glu: C2, δ55.7; C3, δ28; C4, δ34.5), Asp (C2, δ53.2; C3, δ37.5), Suc (C2/C3, δ35), and Tau (C1, δ48.3; C2, δ36.2). The corresponding resonance assignments with chemical shifts of metabolites in ^{13}C NMR spectra are shown in Supplementary Table 1. The PLS-DA score plot illustrates a distinct metabolic separation among Con, DICD, and FGF21-treated mice based on [1-^{13}C]-glucose metabolism (Fig. 5B), and these metabolic differences were ascribed to the glutamate, glutamine, and lactate levels (Fig. 5C).

Figure 6 illustrates [1-^{13}C]-glucose metabolism in brain tissues of Con, DICD, and FGF21-treated mice. Firstly, [1-^{13}C]-glucose was disintegrated into [3-^{13}C]-pyruvate, and pyruvate was then converted either into [3-^{13}C]-alanine through transamination or into [3-^{13}C]-lactate through anaerobic glycolysis. Additionally,

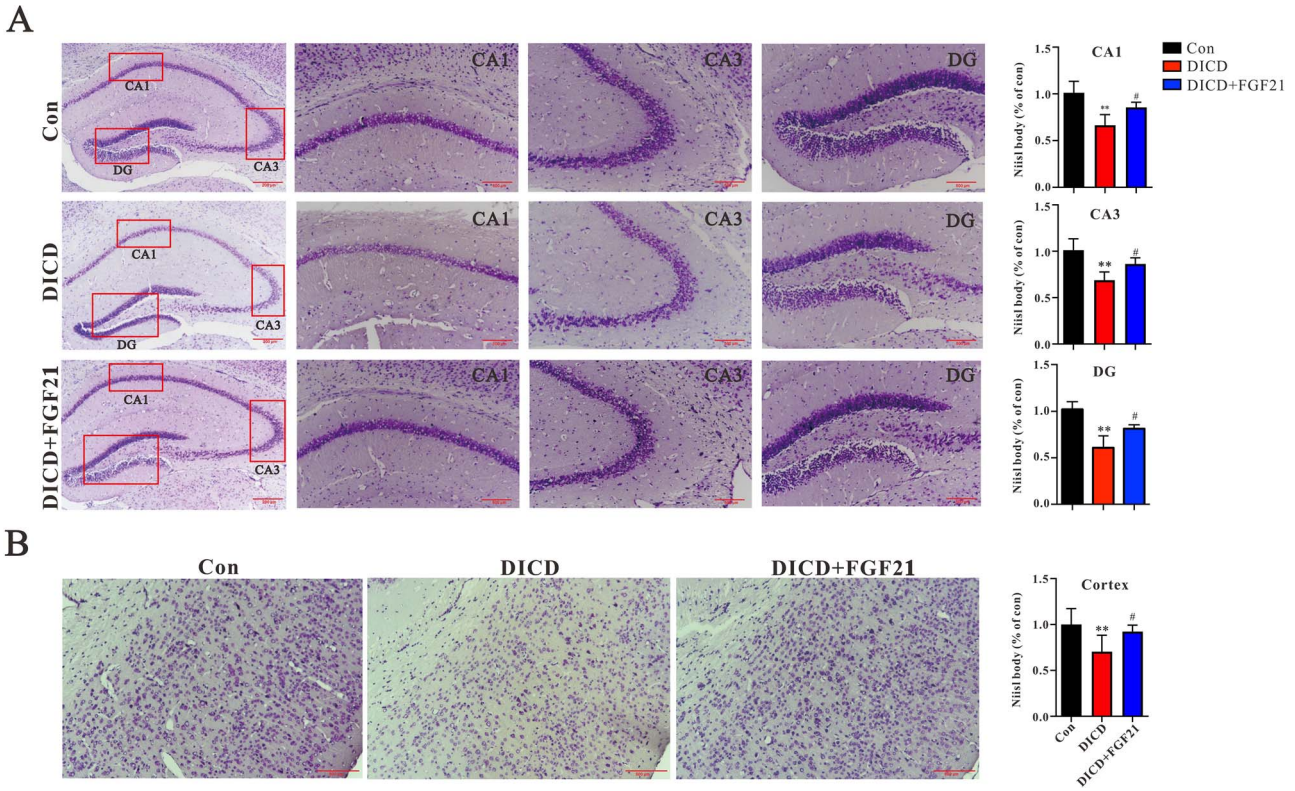

Fig. 2. FGF21 attenuated the neuronal loss in the hippocampi and cortices of the DICD mice. Representative Nissl staining images of (A) hippocampus and (B) cortex tissues of mice and corresponding quantitative results (n = 3). Bar = 500 μm. Data are expressed as the mean ± SD. The significance of difference among three groups was analyzed by using ANOVA with a Bonferroni-adjusted test for pairwise comparisons. Cornu ammonis area 1, CA1; Cornu ammonis area 3, CA3; dentate gyrus, DG.

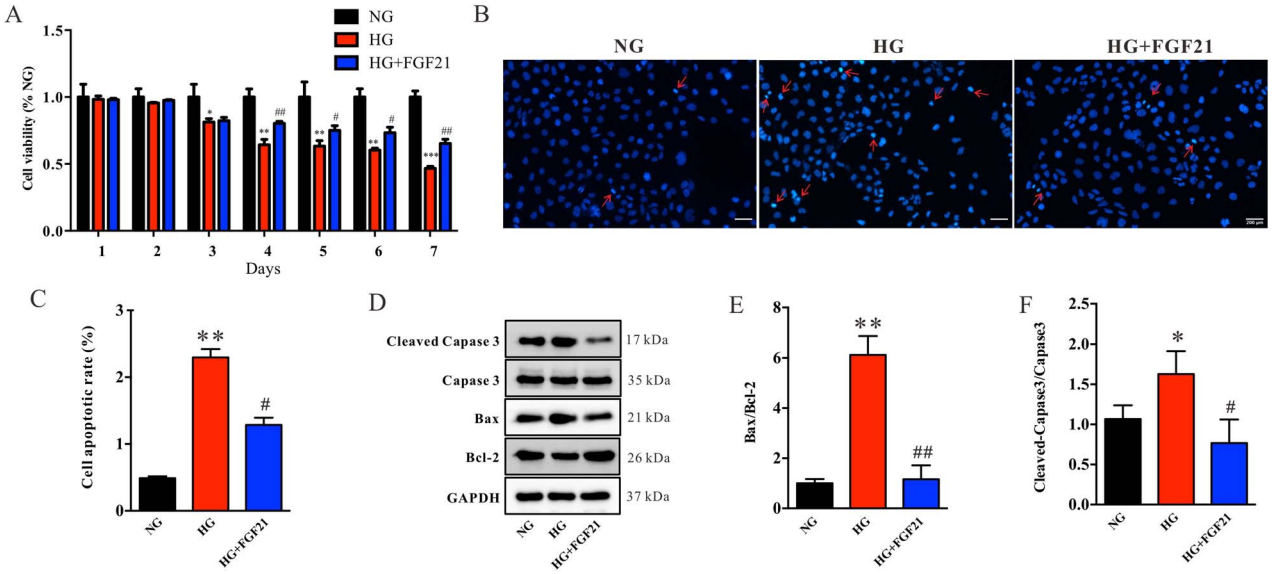

Fig. 3. FGF21 alleviated HG-induced SH-SY5Y cell apoptosis. SH-SY5Y cells were treated with 50-mM glucose for indicated time points (1, 2, 3, 4, 5, 6, and 7 days) in the absence or presence of the treatment with 100 ng/mL FGF21 or 5.5 mM glucose as control, and day 4 was selected as further time points. (A) The CCK-8 assay was conducted to measure cell viability (n = 3). (B, C) Hoechst 33342 nuclear staining was performed to assess cell apoptosis (n = 3). (D) The western blot assay was conducted to determine the Bax, bcl-2, caspase-3, and cleaved caspase-3 protein levels in brain tissues of the normal, DICD, and FGF21-treated mice (n = 3). (E) Bax expression was quantified based on bcl-2 expression. (F) Cleaved caspase-3 expression normalized to caspase-3 expression. Bar = 200 μm. Data are expressed as the mean ± SD. The significance of difference among three groups was analyzed by using ANOVA with a Bonferroni-adjusted test for pairwise comparisons. $^{*}P < 0.05$, $^{**}P < 0.01$, $^{***}P < 0.001$ vs. NG group; $^{\#}P < 0.05$, $^{\#\#}P < 0.01$, $^{\#\#\#}P < 0.001$ vs. HG group.

[3-^{13}C]-pyruvate was metabolized into [3-^{13}C]-oxaloacetate through pyruvate carboxylase or oxidized into [2-^{13}C]-acetyl-CoA through pyruvate dehydrogenase by tricarboxylic acid (TCA) cycle, while inducing [4-^{13}C]-2-oxoglutarate (2-OG) and [2-^{13}C]-2-OG labeling, respectively. Subsequently, [4-^{13}C]-2-OG was transaminated to [4-^{13}C]-glutamate, which might be converted into

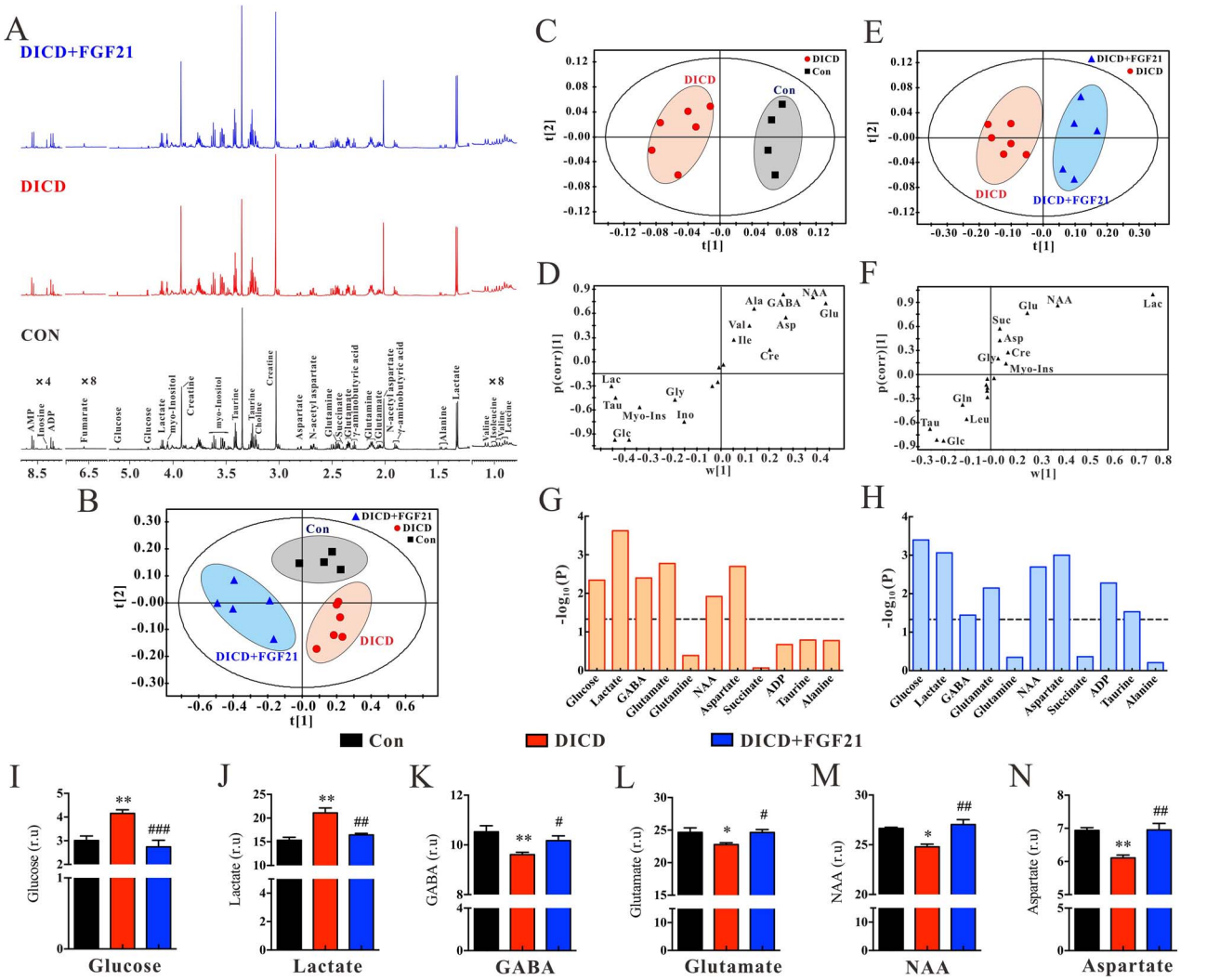

Fig. 4. Metabolic alterations of brain tissues in the DICD mice following FGF21 treatment. (A) Representative 600 MHz ^{1}H-NMR spectra from all three groups of mice. (B) The PLS-DA score plot based on brain metabolomics among the Con, DICD, and FGF21-treated mice. (C) OPLS-DA score plot, (D) corresponding loading plot, and (E) $-\log_{10}$ (P) values between the Con and DICD mice. (F) OPLS-DA score plot, (G) corresponding loading plot, and (H) $-\log_{10}$ (P) values between the DICD and FGF21-treated mice. Changes of (I) glucose, (J) lactate, (K) GABA, (L) glutamate, (M) NAA, and (N) aspartate levels in brain tissues among Con, DICD, and FGF21-treated mice. Data are expressed as the mean ± SD. The significance of difference among three groups was analyzed by using ANOVA with a Bonferroni-adjusted test for pairwise comparisons. $^{*}P < 0.05$, $^{**}P < 0.01$, $^{***}P < 0.001$ vs. normal mice; $^{\#}P < 0.05$, $^{\#\#}P < 0.01$, $^{\#\#\#}P < 0.001$ vs. DICD mice.

[4-^{13}C]-glutamine or decarboxylated into [2-^{13}C]-GABA. In addition, [3-^{13}C]-oxaloacetate and [2-^{13}C]-2-OG were transformed into [2-^{13}C]-glutamine and [2-^{13}C]-glutamate, respectively. [2-^{13}C]-Suc and [2-^{13}C]-Asp were specifically labeled within the initial turn during the TCA cycle. In the second turn, specific labeling with [3-^{13}C]-Asp, [2-^{13}C]-glutamate, [3-^{13}C]-glutamate, [2-^{13}C]-glutamine, [3-^{13}C]-glutamine, [4-^{13}C]-glutamine, [3-^{13}C]-GABA, and [4-^{13}C]-GABA was performed. As shown in Fig. 6, glucose's ^{13}C labeling was more enhanced in DICD mice than Con mice but significantly decreased after FGF21 treatment. To trace the metabolic fate related to glucose metabolism, we observed that [3-^{13}C]-lactate, [3-^{13}C]-Asp, [4-^{13}C]-glutamine, [3-^{13}C]-glutamine, [4-^{13}C]-glutamate, and [4-^{13}C]-GABA enrichment from [1-^{13}C]-glucose distinctly decreased in the DICD mice; however, these trends were markedly reversed after FGF21 treatment. Therefore, these results revealed that disturbances of glucose metabolism and corresponding neurotransmitter metabolism may be related to DICD incidence, which could be markedly restored by i.c.v FGF21 treatment.

FGF21 alleviates DICD-induced metabolic dysfunctions via the PI3K/AKT/GSK3-β pathway

The PI3K/AKT/GSK3-β pathway is a classical pathway responsible for the physiologic hemo-state of glucose metabolism (Chen et al. 2019); thus, we presumed that FGF21 regulated glucose homeostasis in DICD via the PI3K/AKT/GSK3-β pathway. The PI3K, AKT, and GSK3-β phosphorylation levels dramatically declined in the hippocampi (Fig. 7A and B) and cortices (Fig. 7C and D) of DICD mice relative to the levels in those of normal mice, but FGF21 treatment significantly reversed these levels. Hence, our data indicated that the neuroprotective effect of FGF21 on DICD may be mediated by glucose metabolism and corresponding neurotransmitter metabolism via PI3K/AKT/GSK3-β signaling pathway activation (Fig. 8).

Discussion

Diabetes induces CNS damage, causing injury to the structure and function and cognitive dysfunction (Wu et al. 2020). DICD is

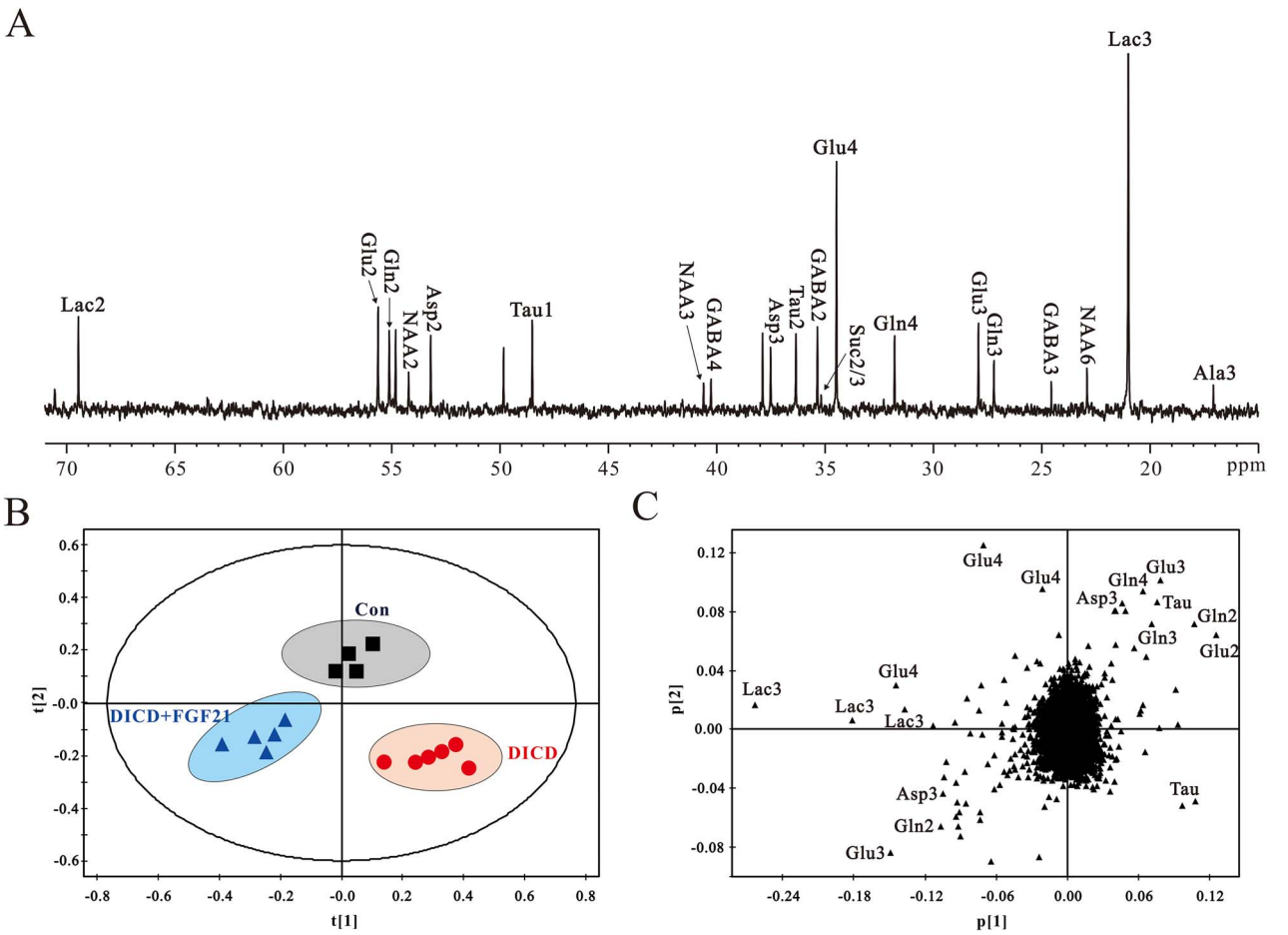

Fig. 5. ^{13}C-NMR metabolomic analysis. (A) Representative ^{13}C-NMR spectrum for brain tissue of the normal mice following [1-^{13}C]-glucose infusion. (B) PLS-DA score and (C) loading plot based on ^{13}C-NMR data. Metabolite abbreviation: Ala, alanine; Lac, lactate; NAA, N-acetyl aspartate; Gln, glutamine; GABA, γ-aminobutyric acid; Tau, taurine; Suc, succinate; Glu, glutamate; Asp, aspartate.

a primary neurodegenerative disease that negatively affects the quality of life of humans. Hence, efficient treatments for DICD are urgently required. In the present study, we identified FGF21 as a possible drug candidate for treating DICD, as characterized by alleviated cognitive impairment, attenuated loss of cortical neurons, and reductions in neuron cell apoptosis. Furthermore, the metabolic mechanism underlying i.c.v FGF21 infusion on DICD was investigated by using ^{1}H NMR-based metabolomics and a ^{13}C NMR approach combined with intravenous [1-^{13}C]-glucose infusion. Metabolomics results demonstrated that the DICD mice exhibited significant metabolic disorders compared with the normal mice; however, i.c.v FGF21 infusion markedly remodeled these metabolic dysfunctions, which are particularly involved in glucose metabolism and neurotransmitter metabolism.

The brain requires a stable energy supply, and disruptive energy metabolism has been linked to accelerated cognitive decline (Belanger et al. 2011). Glucose is considered as an essential brain energy substrate, and ~25% of glucose utilization can be used to maintain the basal brain function (Han et al. 2021). Glucose is disintegrated into pyruvate and then converted to lactate via the anaerobic glycolysis pathway or oxidized via the TCA cycle. In the present study, we discovered the lower ^{13}C incorporation into lactate, alanine, Asp, glutamine, glutamate, and GABA after [1-^{13}C]-glucose infusion in DICD mice relative to those in Con mice, but these decreased trends were reversed after FGF21 treatment, suggesting that FGF21 alleviated DICD-induced inhibition of pyruvate recycling and aberration of neuronal TCA cycle activity. Additionally, lactate is a key energy substrate in the CNS (Barros 2013), and an increase in the lactate level is associated with impaired cognition in humans (Liguori et al. 2015) and animal models (Zhao et al. 2018). We observed significant elevated glucose and lactate contents in the brain of DICD mice relative to those in the normal mice, whereas the glucose and lactate contents were decreased in the DICD mice treated with FGF21. Thus, disruptive glucose and lactate metabolism may suggest that a potential role of FGF21 in regulating energy metabolism during the development of DICD. High levels of lactate and glucose in the brain may enhance glycolytic upregulation. Studies have shown that impaired brain aerobic glycolysis is associated with several major neurodegenerative disorders, such as Alzheimer's disease (Le Douce et al. 2020), Parkinson's disease (Smith et al. 2018), amyotrophic lateral sclerosis (Allen et al. 2014), and Huntington's disease (Vallee et al. 2018). Additionally, brain glucose deficits could be a contributing factor for neurotoxic protein accumulation (Cunnane et al. 2020), brain microvascular endothelial barrier dysfunction (Li et al. 2015) and toxic reactive carbonyl species production (Jomova et al. 2010), indicating a clear link between abnormal glucose metabolism and neurodegenerative disorders. Our results suggested that disruptive glucose metabolism may result in DICD, which could be attenuated by i.c.v FGF21 infusion.

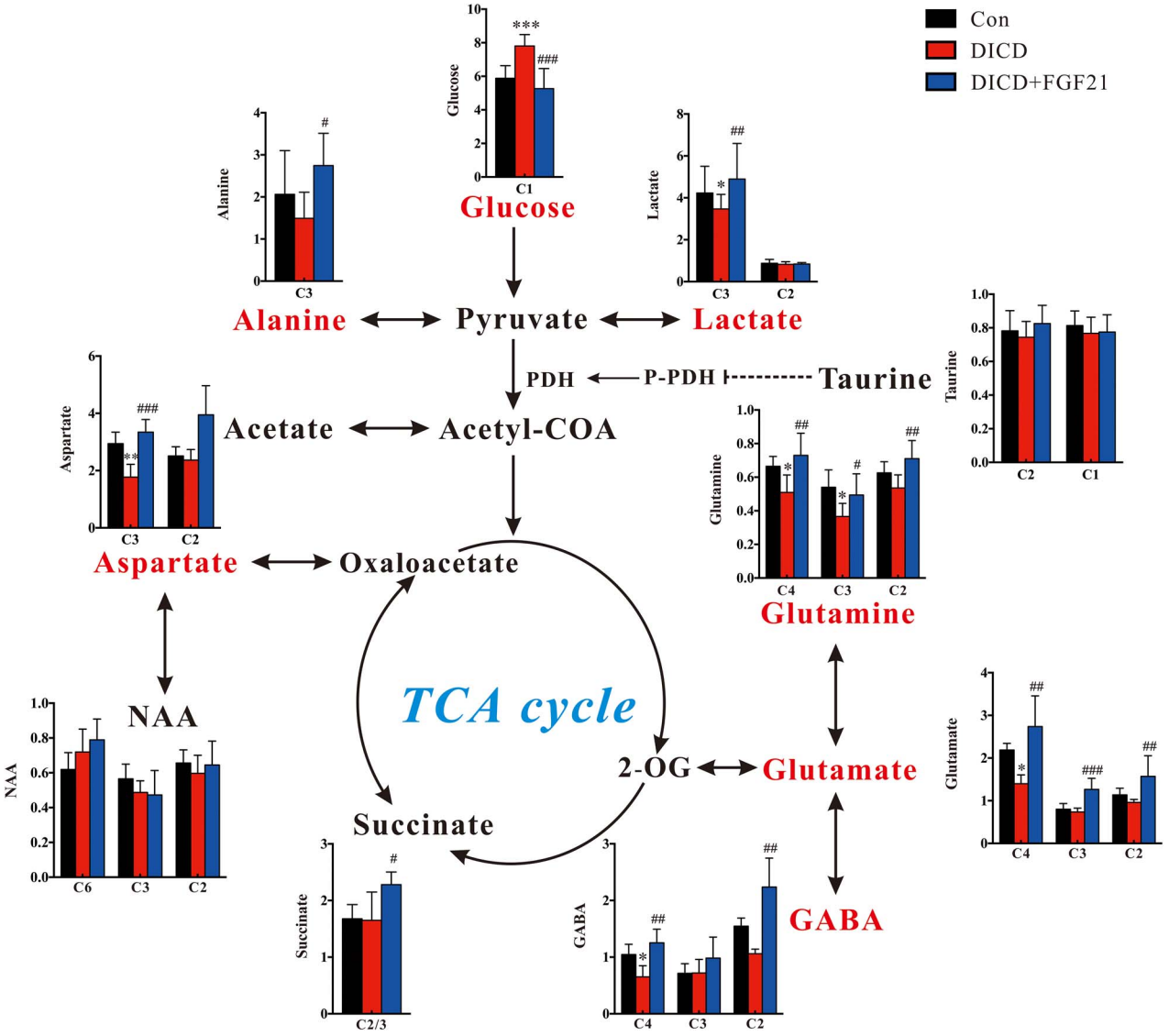

Fig. 6. [1-^{13}C]-glucose metabolic fate of brain tissues among Con, DICD, and FGF21-treated mice. Analysis of metabolic pathways by using the KEGG and SMPDB databases. Data are expressed as the mean ± SD. The significance of difference among three groups was analyzed by using ANOVA with a Bonferroni-adjusted test for pairwise comparisons. $^{*}P < 0.05$, $^{**}P < 0.01$, $^{***}P < 0.001$ vs. normal mice; $^{\#}P < 0.05$, $^{\#\#}P < 0.01$, $^{\#\#\#}P < 0.001$ vs. DICD mice.

Metabonomics results also demonstrated that FGF21 treatment might be involved in regulating neurotransmitter metabolism. Glutamate is a key excitatory neurotransmitter within the CNS and plays a prominent role in the glutamate/GABA-glutamine cycle (GGC) (Bak et al. 2006). In the GGC, glutamate, a precursor for glutamine neurotransmitters, can be indirectly metabolized into the inhibitory neurotransmitter GABA (Bak et al. 2006). The aberrant GGC cycle metabolism is associated with cognitive decline (Myhrer 2003). In this study, significant decreases in the levels of brain glutamate, glutamine, and GABA were observed in DICD mice compared with Con mice. These findings are in line with the disturbances of GGC cycle metabolism in the brain of STZ-induced DM rats (Zheng et al. 2017a; Gao et al. 2019), as well as type 2 diabetic (T2D) mice with cognitive dysfunction (Zheng et al. 2017b; Zheng et al. 2017c). Hence, the disruptive GGC cycle may be related to diabetes-induced cognitive impairment. FGF21 treatment significantly increased glutamate, glutamine, and GABA levels to the normal range, indicating that FGF21 could exert its neuroprotective effect on DICD mice by remodeling GGC metabolism. Asp is another excitatory neurotransmitter synthesized from glucose in the brain (Kolker 2018), which is also related to cognition (Gilmour et al. 2012). Relative to normal mice, DICD mice exhibited a decreased Asp content in the brain, which significantly increased after FGF21 treatment. Collectively, our results demonstrated that FGF21's neuroprotective efficacy in DICD could be achieved by regulating neurotransmitter metabolism.

NAA is considered as a marker of neuronal viability (Moffett et al. 2007), and several studies have identified a correlation between the decreased NAA levels and cognitive deficits (Chao et al. 2005; Rigotti et al. 2007). Our results demonstrated that the DICD mice had a lower level of NAA compared with the normal mice; however, the NAA level was increased remarkably after FGF21 treatment, suggesting that the protective effect of FGF21 on DICD may be associated with the recovery of NAA-associated neuronal loss. On the other hand, NAA is a neuron-specific metabolite synthesized from an excitatory neurotransmitter (Baslow 2003), which helps explain [6-^{13}C]-NAA, [3-^{13}C]-NAA,

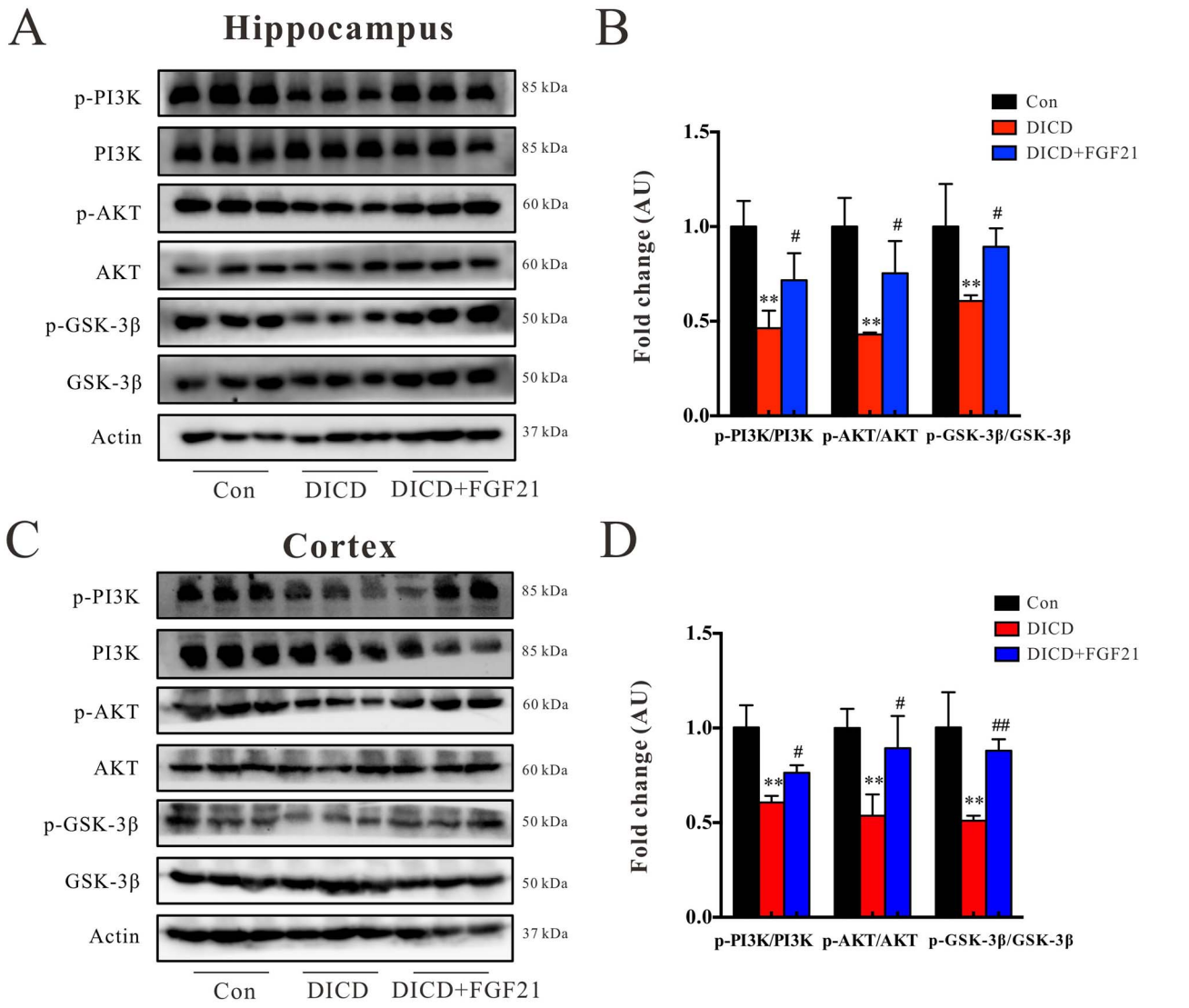

Fig. 7. FGF21 treatment significantly activated DICD-mediated PI3K/AKT/GSK-3β pathway suppression. (A) Western blotting and (B) quantitative analysis of p-GSK-3β, GSK-3β, p-AKT, AKT, and p-PI3K, PI3K expressions in the hippocampus of mice. (C) Western blot and (D) quantitative analysis of p-GSK-3β, GSK-3β, p-AKT, and AKT expressions in the cortex of mice. Data are expressed as the mean ± SD. The significance of difference among three groups was analyzed by using ANOVA with a Bonferroni-adjusted test for pairwise comparisons. $^{*}P < 0.05$, $^{**}P < 0.01$, $^{***}P < 0.001$ vs. normal mice; $^{\#}P < 0.05$, $^{\#\#}P < 0.01$, $^{\#\#\#}P < 0.001$ vs. DICD mice.

and [2-^{13}C]-NAA enrichment from [1-^{13}C]-glucose were invariant in DICD.

The PI3K/AKT/GSK-3β pathway is a critical insulin signaling pathway for glucose regulation (Yin et al. 2017). Under normal conditions, insulin is an upstream regulator for the PI3K/AKT pathway in the brain, and the activation of phosphorylated GSK-3β promotes glucose utilization and regulates energy metabolism (Arnold et al. 2018). Numerous studies have suggested the crucial function of the PI3K/AKT/GSK-3β pathway in maintaining neuronal functions (Chiu and Cline 2010; Cho et al. 2014; Malemud 2015). Coordinating with the alterations of brain glucose and neurotransmitter metabolism, the PI3K/AKT/GSK-3β pathway was remarkably inhibited in the hippopotamus and cortex of the DICD mice compared with normal mice, but significantly activated by i.c.v FGF21 treatment. Studies have demonstrated that promoting dysregulation of the PI3K/AKT signaling pathway is a promising strategy to ameliorate cognitive decline in the STZ-mediated DM rats (Bathina and Das 2018) and db/db mice (Wu et al. 2020). Hence, we speculate that FGF21 effectively suppressed diabetes-induced neuronal loss and apoptosis, improved brain glucose homeostasis and neurotransmitter metabolism, and ameliorated cognitive deficits in DICD mice by activating the PI3K/AKT/GSK-3β pathway.

The present study investigated the biological effects of a single i.c.v. dose of FGF21 on DICD, with a specific focus on the observation period of 2 wk subsequent to FGF21 injection. Nevertheless, as a chronic disease, FGF21-based treatment may require prolonged and continuous medication in DICD. Hence, different time-points of experiments would be recommended for elucidating the long-term pharmaceutical effect of FGF21 on DICD in a future study. In conclusion, the current study proved that a single i.c.v injection of FGF21 effectively ameliorated cognitive impairment and suppressed neuronal loss and apoptosis of DICD mice in a short-time period, which possibly by remodeling glucose metabolism and neurotransmitter metabolism via PI3K/AKT/GSK-3β signaling pathway activation. Thus, we believe

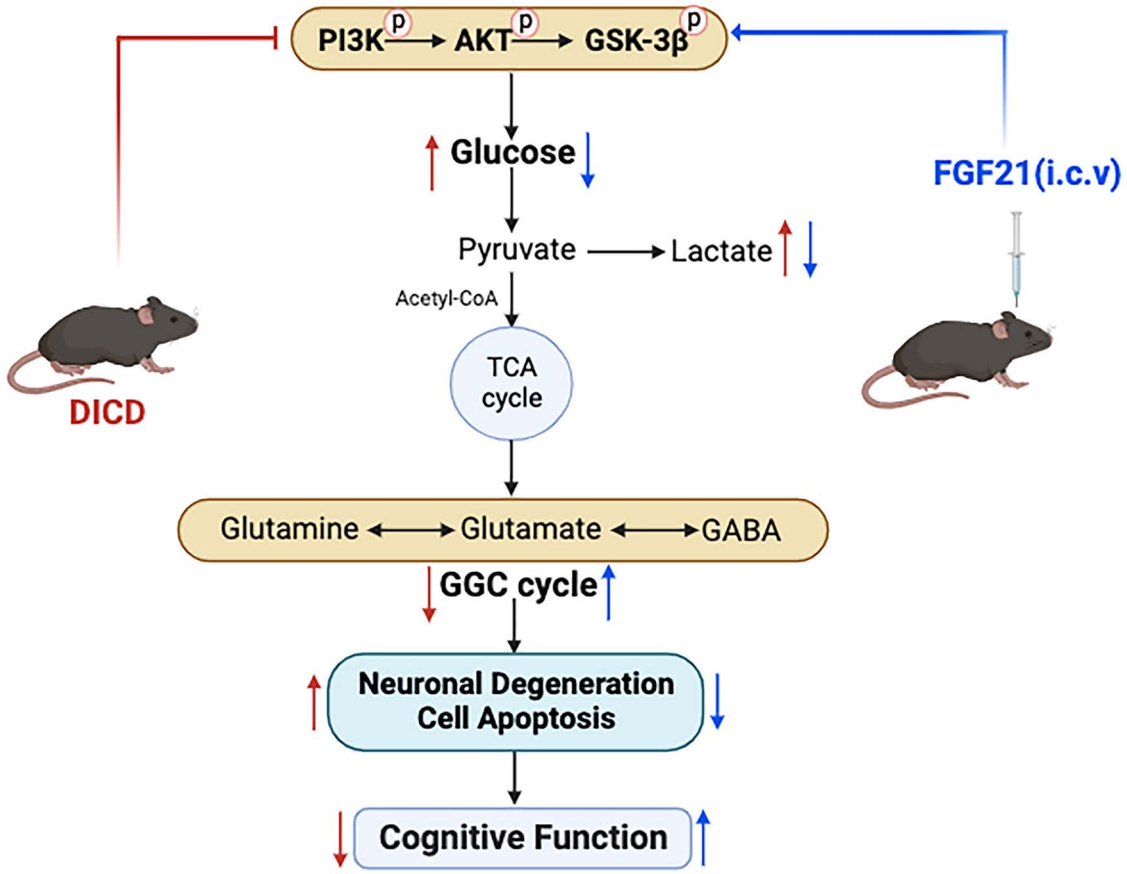

Fig. 8. Possible metabolic mechanism of FGF21 in preventing DICD: FGF21 effectively suppressed diabetes-induced neuronal loss and apoptosis, improved brain glucose homeostasis and neurotransmitter metabolism, and consequently ameliorated cognitive deficits of DICD mice, possibly by activating the PI3K/AKT/GSK-3β signaling pathway. Red arrow indicates changes in DICD, and blue arrow indicates changes after i.c.v FGF21 infusion.

our results may offer insights into the therapeutic interventions for DICD.

Acknowledgments

BioRender.com was used to create mechanism illustrations in Fig. 8. The Scientific Research Center of Wenzhou Medical University is acknowledged for technical services.

Supplementary material

Supplementary material is available at *Cerebral Cortex* online.

Author contributions

Xi Zhang (Data curation, Formal analysis, Visualization, Writing—original draft), Hong Zheng (Conceptualization, Supervision, Validation), Zhitao Ni (Methodology, Visualization), Yuyin Shen (Data curation, Writing—review & editing), Wenqing Li (Investigation, Software), Liangcai Zhao (Investigation, Resources), Chen Li (Funding acquisition, Project administration, Supervision), and Hongchang Gao (Funding acquisition, Project administration, Writing—review & editing).

Funding

This work was supported by the National Natural Science Foundation of China (Nos. 21974096, 82000384).

Conflict of interest statement: None declared.

Data availability

The datasets used and analyzed during the current study are available from the corresponding author on reasonable request.

References

Adams AC, Cheng CC, Coskun T, Kharitonenkov A. Fgf21 requires betaklotho to act in vivo. *PLoS One*. 2012:7(11):e49977.

Allen SP, Rajan S, Duffy L, Mortiboys H, Higginbottom A, Grierson AJ, Shaw PJ. Superoxide dismutase 1 mutation in a cellular model of amyotrophic lateral sclerosis shifts energy generation from oxidative phosphorylation to glycolysis. *Neurobiol Aging*. 2014:35(6):1499–1509.

Arnold SE, Arvanitakis Z, Macauley-Rambach SL, Koenig AM, Wang HY, Ahima RS, Craft S, Gandy S, Buettner C, Stoeckel LE et al. Brain insulin resistance in type 2 diabetes and alzheimer disease: Concepts and conundrums. *Nat Rev Neurol*. 2018:14(3):168–181.

Bak LK, Schousboe A, Waagepetersen HS. The glutamate/gaba-glutamine cycle: Aspects of transport, neurotransmitter homeostasis and ammonia transfer. *J Neurochem*. 2006:98(3):641–653.

Barros LF. Metabolic signaling by lactate in the brain. *Trends Neurosci*. 2013:36(7):396–404.

Baslow MH. N-acetylaspartate in the vertebrate brain: Metabolism and function. *Neurochem Res*. 2003:28(6):941–953.

Bathina S, Das UN. Dysregulation of pi3k-akt-mtor pathway in brain of streptozotocin-induced type 2 diabetes mellitus in wistar rats. *Lipids Health Dis*. 2018:17(1):168.

Belanger M, Allaman I, Magistretti PJ. Brain energy metabolism: Focus on astrocyte-neuron metabolic cooperation. *Cell Metab.* 2011:14(6):724–738.

BonDurant LD, Potthoff MJ. Fibroblast growth factor 21: A versatile regulator of metabolic homeostasis. *Annu Rev Nutr.* 2018:38(1): 173–196.

Brismar T, Maurex L, Cooray G, Juntti-Berggren L, Lindstrom P, Ekberg K, Adner N, Andersson S. Predictors of cognitive impairment in type 1 diabetes. *Psychoneuroendocrinology.* 2007:32(8–10): 1041–1051.

Byun S, Seok S, Kim YC, Zhang Y, Yau P, Iwamori N, Xu HE, Ma J, Kemper B, Kemper JK. Fasting-induced fgf21 signaling activates hepatic autophagy and lipid degradation via jmjd3 histone demethylase. *Nat Commun.* 2020:11(1):807.

Chao LL, Schuff N, Kramer JH, Du AT, Capizzano AA, O'Neill J, Wolkowitz OM, Jagust WJ, Chui HC, Miller BL, et al. Reduced medial temporal lobe n-acetylaspartate in cognitively impaired but nondemented patients. *Neurology.* 2005:64(2):282–289.

Chao CC, Gutierrez-Vazquez C, Rothhammer V, Mayo L, Wheeler MA, Tjon EC, Zandee SEJ, Blain M, de Lima KA, Takenaka MC, et al. Metabolic control of astrocyte pathogenic activity via cpla2-mavs. *Cell.* 2019:179(7):1483–1498 e1422.

Chen T, Zhang Y, Liu Y, Zhu D, Yu J, Li G, Sun Z, Wang W, Jiang H, Hong Z. Mir-27a promotes insulin resistance and mediates glucose metabolism by targeting ppar-gamma-mediated pi3k/akt signaling. *Aging (Albany NY).* 2019:11(18):7510–7524.

Chiu SL, Cline HT. Insulin receptor signaling in the development of neuronal structure and function. *Neural Dev.* 2010:5(1):7.

Cho YR, Lim JH, Kim MY, Kim TW, Hong BY, Kim YS, Chang YS, Kim HW, Park CW. Therapeutic effects of fenofibrate on diabetic peripheral neuropathy by improving endothelial and neural survival in db/db mice. *PLoS One.* 2014:9(1):e83204.

Choi YS, Song JE, Lee JE, Kim E, Kim CH, Kim DH, Song HT. Hyperpolarized [1-13c]lactate flux increased in the hippocampal region in diabetic mice. *Mol Brain.* 2019:12(1):88.

Cui Y, Yang M, Wang Y, Ren J, Lin P, Cui C, Song J, He Q, Hu H, Wang K, et al. Melatonin prevents diabetes-associated cognitive dysfunction from microglia-mediated neuroinflammation by activating autophagy via tlr4/akt/mtor pathway. *FASEB J.* 2021:35(4):e21485.

Cunnane SC, Trushina E, Morland C, Prigione A, Casadesus G, Andrews ZB, Beal MF, Bergersen LH, Brinton RD, de la Monte S, et al. Brain energy rescue: An emerging therapeutic concept for neurodegenerative disorders of ageing. *Nat Rev Drug Discov.* 2020:19(9):609–633.

Dutchak PA, Katafuchi T, Bookout AL, Choi JH, Yu RT, Mangelsdorf DJ, Kliewer SA. Fibroblast growth factor-21 regulates ppargamma activity and the antidiabetic actions of thiazolidinediones. *Cell.* 2012:148(3):556–567.

Gaich G, Chien JY, Fu H, Glass LC, Deeg MA, Holland WL, Kharitonenkov A, Bumol T, Schilske HK, Moller DE. The effects of ly2405319, an fgf21 analog, in obese human subjects with type 2 diabetes. *Cell Metab.* 2013:18(3):333–340.

Gao H, Jiang Q, Ji H, Ning J, Li C, Zheng H. Type 1 diabetes induces cognitive dysfunction in rats associated with alterations of the gut microbiome and metabolomes in serum and hippocampus. *Biochim Biophys Acta Mol Basis Dis.* 2019:1865(12):165541.

Geng L, Lam KSL, Xu A. The therapeutic potential of fgf21 in metabolic diseases: From bench to clinic. *Nat Rev Endocrinol.* 2020:16(11):654–667.

Gilmour G, Dix S, Fellini L, Gastambide F, Plath N, Steckler T, Talpos J, Tricklebank M. NMDA receptors, cognition and schizophrenia—testing the validity of the NMDA receptor hypofunction hypothesis. *Neuropharmacology.* 2012:62(3):1401–1412.

Han R, Liang J, Zhou B. Glucose metabolic dysfunction in neurodegenerative diseases-new mechanistic insights and the potential of hypoxia as a prospective therapy targeting metabolic reprogramming. *Int J Mol Sci.* 2021:22(11):5887.

Hsuchou H, Pan W, Kastin AJ. The fasting polypeptide fgf21 can enter brain from blood. *Peptides.* 2007:28(12):2382–2386.

Ivanisevic J, Siuzdak G. The role of metabolomics in brain metabolism research. *J Neuroimmune Pharmacol.* 2015:10(3): 391–395.

Jomova K, Vondrakova D, Lawson M, Valko M. Metals, oxidative stress and neurodegenerative disorders. *Mol Cell Biochem.* 2010:345(1–2): 91–104.

Kang K, Xu P, Wang M, Chunyu J, Sun X, Ren G, Xiao W, Li D. Fgf21 attenuates neurodegeneration through modulating neuroinflammation and oxidant-stress. *Biomed Pharmacother.* 2020:129:110439.

Kharitonenkov A, Wroblewski VJ, Koester A, Chen YF, Clutinger CK, Tigno XT, Hansen BC, Shanafelt AB, Etgen GJ. The metabolic state of diabetic monkeys is regulated by fibroblast growth factor-21. *Endocrinology.* 2007:148(2):774–781.

Kolker S. Metabolism of amino acid neurotransmitters: The synaptic disorder underlying inherited metabolic diseases. *J Inherited Metab Dis.* 2018:41(6):1055–1063.

Kong FJ, Ma LL, Guo JJ, Xu LH, Li Y, Qu S. Endoplasmic reticulum stress/autophagy pathway is involved in diabetes-induced neuronal apoptosis and cognitive decline in mice. *Clin Sci (Lond).* 2018:132(1):111–125.

Le Douce J, Maugard M, Veran J, Matos M, Jego P, Vigneron PA, Faivre E, Toussay X, Vandenberghe M, Balbastre Y, et al. Impairment of glycolysis-derived l-serine production in astrocytes contributes to cognitive deficits in alzheimer's disease. *Cell Metab.* 2020:31(3):503–517 e508.

Li W, Maloney RE, Aw TY. High glucose, glucose fluctuation and carbonyl stress enhance brain microvascular endothelial barrier dysfunction: Implications for diabetic cerebral microvasculature. *Redox Biol.* 2015:5:80–90.

Liguori C, Stefani A, Sancesario G, Sancesario GM, Marciani MG, Pierantozzi M. Csf lactate levels, tau proteins, cognitive decline: A dynamic relationship in alzheimer's disease. *J Neurol Neurosurg Psychiatry.* 2015:86(6):655–659.

Lin Z, Tian H, Lam KS, Lin S, Hoo RC, Konishi M, Itoh N, Wang Y, Bornstein SR, Xu A, et al. Adiponectin mediates the metabolic effects of fgf21 on glucose homeostasis and insulin sensitivity in mice. *Cell Metab.* 2013:17(5):779–789.

Malemud CJ. The pi3k/akt/pten/mtor pathway: A fruitful target for inducing cell death in rheumatoid arthritis? *Future Med Chem.* 2015:7(9):1137–1147.

Moffett JR, Ross B, Arun P, Madhavarao CN, Namboodiri AM. N-acetylaspartate in the cns: From neurodiagnostics to neurobiology. *Prog Neurobiol.* 2007:81(2):89–131.

Musen G, Tinsley LJ, Marcinkowski KA, Pober D, Sun JK, Khatri M, Huynh R, Lu A, King GL, Keenan HA. Cognitive function deficits associated with long-duration type 1 diabetes and vascular complications. *Diabetes Care.* 2018:41(8):1749–1756.

Myhrer T. Neurotransmitter systems involved in learning and memory in the rat: A meta-analysis based on studies of four behavioral tasks. *Brain Res Brain Res Rev.* 2003:41(2–3): 268–287.

Ngo CQ, Chai R, Jones TW, Nguyen HT. Electroencephalogram reactivity to hyperglycemia in patients with type 1 diabetes. *Annu Int Conf IEEE Eng Med Biol Soc.* 2020:2020:5224–5227.

Nicholson JK, Lindon JC, Holmes E. 'Metabonomics': Understanding the metabolic responses of living systems to pathophysiological

stimuli via multivariate statistical analysis of biological nmr spectroscopic data. *Xenobiotica*. 1999:29(11):1181–1189.

Ransohoff RM. How neuroinflammation contributes to neurodegeneration. *Science*. 2016:353(6301):777–783.

Rigotti DJ, Inglese M, Gonen O. Whole-brain n-acetylaspartate as a surrogate marker of neuronal damage in diffuse neurologic disorders. *AJNR Am J Neuroradiol*. 2007:28(10):1843–1849.

Sa-Nguanmoo P, Tanajak P, Kerdphoo S, Satjaritanun P, Wang X, Liang G, Li X, Jiang C, Pratchayasakul W, Chattipakorn N, et al. Fgf21 improves cognition by restored synaptic plasticity, dendritic spine density, brain mitochondrial function and cell apoptosis in obese-insulin resistant male rats. *Horm Behav*. 2016:85:86–95.

Santoso P, Nakata M, Shiizaki K, Boyang Z, Parmila K, Otgon-Uul Z, Hashimoto K, Satoh T, Mori M, Kuro OM, et al. Fibroblast growth factor 21, assisted by elevated glucose, activates paraventricular nucleus nucb2/nesfatin-1 neurons to produce satiety under fed states. *Sci Rep*. 2017:7(1):45819.

Scarlett JM, Rojas JM, Matsen ME, Kaiyala KJ, Stefanovski D, Bergman RN, Nguyen HT, Dorfman MD, Lantier L, Wasserman DH, et al. Central injection of fibroblast growth factor 1 induces sustained remission of diabetic hyperglycemia in rodents. *Nat Med*. 2016:22(7):800–806.

Shulman GI, Rothman DL, Jue T, Stein P, DeFronzo RA, Shulman RG. Quantitation of muscle glycogen synthesis in normal subjects and subjects with non-insulin-dependent diabetes by 13c nuclear magnetic resonance spectroscopy. *New Engl J Med*. 1990:322(4):223–228.

Smith AM, Depp C, Ryan BJ, Johnston GI, Alegre-Abarrategui J, Evetts S, Rolinski M, Baig F, Ruffmann C, Simon AK, et al. Mitochondrial dysfunction and increased glycolysis in prodromal and early parkinson's blood cells. *Mov Disord*. 2018:33(10):1580–1590.

Vallee A, Lecarpentier Y, Guillevin R, Vallee JN. Aerobic glycolysis in amyotrophic lateral sclerosis and huntington's disease. *Rev Neurosci*. 2018:29(5):547–555.

Veniant MM, Komorowski R, Chen P, Stanislaus S, Winters K, Hager T, Zhou L, Wada R, Hecht R, Xu J. Long-acting fgf21 has enhanced efficacy in diet-induced obese mice and in obese rhesus monkeys. *Endocrinology*. 2012:153(9):4192–4203.

Wang N, Zhao LC, Zheng YQ, Dong MJ, Su Y, Chen WJ, Hu ZL, Yang YJ, Gao HC. Alteration of interaction between astrocytes and neurons in different stages of diabetes: A nuclear magnetic resonance study using [1-(13)c]glucose and [2-(13)c]acetate. *Mol Neurobiol*. 2015:51(3):843–852.

Watanabe H, Miyahisa M, Chikamatsu M, Nishida K, Minayoshi Y, Takano M, Ichimizu S, Kobashigawa Y, Morioka H, Maeda H, et al. Development of a long acting fgf21 analogue-albumin fusion protein and its anti-diabetic effects. *J Controlled Release*. 2020:324:522–531.

Wishart DS, Feunang YD, Marcu A, Guo AC, Liang K, Vazquez-Fresno R, Sajed T, Johnson D, Li C, Karu N, et al. Hmdb 4.0: The human metabolome database for 2018. *Nucleic Acids Res*. 2018:46(D1):D608–D617.

Wu Y, Ye L, Yuan Y, Jiang T, Guo X, Wang Z, Xu K, Xu Z, Liu Y, Zhong X, et al. Autophagy activation is associated with neuroprotection in diabetes-associated cognitive decline. *Aging Dis*. 2019:10(6):1233–1245.

Wu Y, Wu C, Ye L, Wang B, Yuan Y, Liu Y, Zheng P, Xiong J, Li Y, Jiang T, et al. Exogenous fibroblast growth factor 1 ameliorates diabetes-induced cognitive decline via coordinately regulating pi3k/akt signaling and perk signaling. *Cell Commun Signal*. 2020:18(1):81.

Xiong F, Gong K, Xu H, Tu Y, Lu J, Zhou Y, He W, Li W, Li C, Zhao L, et al. Optimized integration of metabolomics and lipidomics reveals brain region-specific changes of oxidative stress and neuroinflammation in type 1 diabetic mice with cognitive decline. *J Adv Res*. 2023:43:233–245.

Xu J, Stanislaus S, Chinookoswong N, Lau YY, Hager T, Patel J, Ge H, Weiszmann J, Lu SC, Graham M, et al. Acute glucose-lowering and insulin-sensitizing action of FGF21 in insulin-resistant mouse models—association with liver and adipose tissue effects. *Am J Physiol Endocrinol Metab*. 2009:297(5):E1105–E1114.

Ye L, Wang X, Cai C, Zeng S, Bai J, Guo K, Fang M, Hu J, Liu H, Zhu L, et al. Fgf21 promotes functional recovery after hypoxic-ischemic brain injury in neonatal rats by activating the pi3k/akt signaling pathway via fgfr1/beta-klotho. *Exp Neurol*. 2019:317:34–50.

Yin X, Xu Z, Zhang Z, Li L, Pan Q, Zheng F, Li H. Association of pi3k/akt/mtor pathway genetic variants with type 2 diabetes mellitus in chinese. *Diabetes Res Clin Pract*. 2017:128:127–135.

Zhang M, Yan W, Yu Y, Cheng J, Yi X, Guo T, Liu N, Shang J, Wang Z, Hu H, et al. Liraglutide ameliorates diabetes-associated cognitive dysfunction via rescuing autophagic flux. *J Pharmacol Sci*. 2021:147(3):234–244.

Zhao L, Dong M, Ren M, Li C, Zheng H, Gao H. Metabolomic analysis identifies lactate as an important pathogenic factor in diabetes-associated cognitive decline rats. *Mol Cell Proteomics*. 2018:17(12):2335–2346.

Zhao L, Jiang H, Xie J, Shen D, Yi Q, Yan J, Li C, Zheng H, Gao H. Effects of fibroblast growth factor 21 on lactate uptake and usage in mice with diabetes-associated cognitive decline. *Mol Neurobiol*. 2022:59(9):5656–5672.

Zheng H, Lin Q, Wang D, Xu P, Zhao L, Hu W, Bai G, Yan Z, Gao H. Nmr-based metabolomics reveals brain region-specific metabolic alterations in streptozotocin-induced diabetic rats with cognitive dysfunction. *Metab Brain Dis*. 2017a:32(2):585–593.

Zheng H, Zheng Y, Wang D, Cai A, Lin Q, Zhao L, Chen M, Deng M, Ye X, Gao H. Analysis of neuron-astrocyte metabolic cooperation in the brain of db/db mice with cognitive decline using 13c nmr spectroscopy. *J Cereb Blood Flow Metab*. 2017b:37(1):332–343.

Zheng H, Zheng Y, Zhao L, Chen M, Bai G, Hu Y, Hu W, Yan Z, Gao H. Cognitive decline in type 2 diabetic db/db mice may be associated with brain region-specific metabolic disorders. *Biochim Biophys Acta Mol Basis Dis*. 2017c:1863(1):266–273.

Zheng H, Ni Z, Cai A, Zhang X, Chen J, Shu Q, Gao H. Balancing metabolome coverage and reproducibility for untargeted nmr-based metabolic profiling in tissue samples through mixture design methods. *Anal Bioanal Chem*. 2018a:410(29):7783–7792.

Zheng T, Liu H, Qin L, Chen B, Zhang X, Hu X, Xiao L, Qin S. Oxidative stress-mediated influence of plasma dpp4 activity to bdnf ratio on mild cognitive impairment in elderly type 2 diabetic patients: Results from the gdmd study in china. *Metabolism*. 2018b:87:105–112.

Zheng H, Xu P, Jiang Q, Xu Q, Zheng Y, Yan J, Ji H, Ning J, Zhang X, Li C, et al. Depletion of acetate-producing bacteria from the gut microbiota facilitates cognitive impairment through the gut-brain neural mechanism in diabetic mice. *Microbiome*. 2021:9(1):145.

Zhou Q, Zheng H, Chen J, Li C, Du Y, Xia H, Gao H. Metabolic fate of glucose in the brain of app/ps1 transgenic mice at 10 months of age: A (13)c nmr metabolomic study. *Metab Brain Dis*. 2018:33(5):1661–1668.